doi:10.26443/seismica.v3i2.1151

Seismic site conditions of RESNOM network

Lenin Ávila-Barrientos * [1,2], **Luis A. Yegres-Herrera** [2], **Hortencia Flores-Estrella** [3], **M. Alejandra Nuñez-Leal** [2], **Hector Gonzalez-Huizar** [2]

[1]Dirección Adjunta de Investigación Humanística y Científica, CONAHCYT, Av. Insurgentes Sur 1582, Col. Crédito Constructor, Alcaldía Benito Juárez, C. P. 03940, Ciudad de México, México, [2]Centro de Investigación Científica y de Educación Superior de Ensenada, Baja California. División de Ciencias de la Tierra, Departamento de Sismología. Carretera Ensenada – Tijuana No. 3918, Zona Playitas, C. P. 22860, Ensenada, Baja California, México, [3]Geothermie Neubrandenburg GmbH, Berliner Straße 40, 13507 Berlin, Germany

Author contributions: *Conceptulaization*: L. Ávila-Barrientos. *Data Curation*: L. Ávila-Barrientos, L. A. Yegres-Herrera. *Formal Analysis*: L. Ávila-Barrientos, L. A. Yegres-Herrera, H. Flores-Estrella, A. Nuñez-Leal. *Methodology*: H. Flores-Estrella. *Writing – original draft*: L. Ávila-Barrientos. *Writing – review & editing*: L. Ávila-Barrientos, L. A. Yegres-Herrera, H. Flores-Estrella, A. Nuñez-Leal, H. Gonzalez-Huizar.

Abstract The Northwest Seismic Network of Mexico (RESNOM) is operated by personnel from the Center for Scientific Research and Higher Education of Ensenada, Baja California (CICESE), which supervises station installation, improvement, and maintenance. We employed seismic noise and the Horizontal to Vertical Spectral Ratio (HVSR) method to determine, for each station, the following site condition parameters: the depth of the rock layer (H_{eng_bed}) and the geotechnical parameter V_{S30}, obtained from 1D shear wave velocity models. Other parameters such as the fundamental frequency (f_0) and the average amplitude at the fundamental frequency (A_0) were also estimated. Our results show clear differences between the values obtained for the Mexicali Valley and the Peninsular ranges regions. The V_{S30} obtained for stations of the Mexicali Valley region falls in the range from 173 m/s to 535 m/s, while for the Peninsular Ranges region it is between 213 m/s and 958 m/s. Regarding the H_{eng_bed} parameter, the values are similar between both regions, from 23 m to 850 m for the Peninsular and from 42 m to 926 m for the Mexicali Valley. Additionally, from the V_{S30} values, we propose the site classification according to the U.S. National Earthquake Hazards Reduction Program (NEHRP).

Production Editor: Gareth Funning
Handling Editor: Pablo Heresi
Copy & Layout Editor: Ethan Williams

Received: November 14, 2023
Accepted: September 11, 2024
Published: October 21, 2024

Non-technical summary Seismic station characterization provides information about the seismic conditions of subsoil. The spatial distribution of these seismic conditions could have implications for seismic hazard assessment. The Northwest Seismic Network of Mexico (RESNOM) is operated by the Center for Scientific Research and Higher Education of Ensenada, Baja California (CICESE) personnel. We employed seismic noise and the Horizontal to Vertical Spectral Ratio (HVSR) method to determine the site condition parameters for each RESNOM station. Our results show clear differences between the values obtained for the Mexicali Valley and the Peninsular Ranges regions. From the V_{S30} values (which is an important geotechnical parameter), we propose the site classification of the stations according to the U.S. National Earthquake Hazards Reduction Program (NEHRP).

1 Introduction

The *Red Sismica del Noroeste de Mexico*, RESNOM, is a seismic network belonging to the *Centro de Investigación Científica y de Educación Superior de Ensenada, Baja California* (CICESE). Since RESNOM was created in 1978, CICESE has been responsible for installing, improving, and monitoring the seismic stations (Zúñiga and Castro, 2005). It was designed to detect, record, and catalog the seismic activity in the north-western part of Mexico, specifically in northern Baja California and northwestern Sonora. The seismic activity in this region is caused mainly by the interaction between the North American and the Pacific tectonic plates, where the recorded earthquakes go from M ~1 microquakes to $M \geq 7.0$ events, e.g., the M_W 7.2, El Mayor-Cucapah earthquake, which occurred on April 10th, 2010 (Hauksson et al., 2010).

The site conditions are defined mainly by the subsoil mechanical properties at each site (Tramelli et al., 2010; Nogoshi and Igarashi, 1971; Flores-Estrella, 2001). They are a key element of the ground motion characteristics and how this can be modified in terms of amplitude, duration, and frequency content. The site conditions, also known as site effects, have a significant impact on hazard and risk assessments (Cornou and Bard, 2019; Cultrera et al., 2021).

The availability of site characterization for seismic stations has recently become an important analysis subject, mainly because of the worldwide increment in seismic networks (Cornou and Bard, 2019; Cultrera et al., 2021; Giulio et al., 2021). According to different studies (Bergamo et al., 2019; Cultrera et al., 2021; Giulio et al., 2021, among others), the optimal parameters to characterize the site conditions are: the fundamental frequency, f_0; the shear wave velocity V_S profile (i.e., shear wave velocity variation with depth); the time-average of V_S over the upper 30 m, V_{S30}; the depth to bedrock, H_{eng_bed}; as well as the surface geology.

*Corresponding author: lenavila@cicese.mx

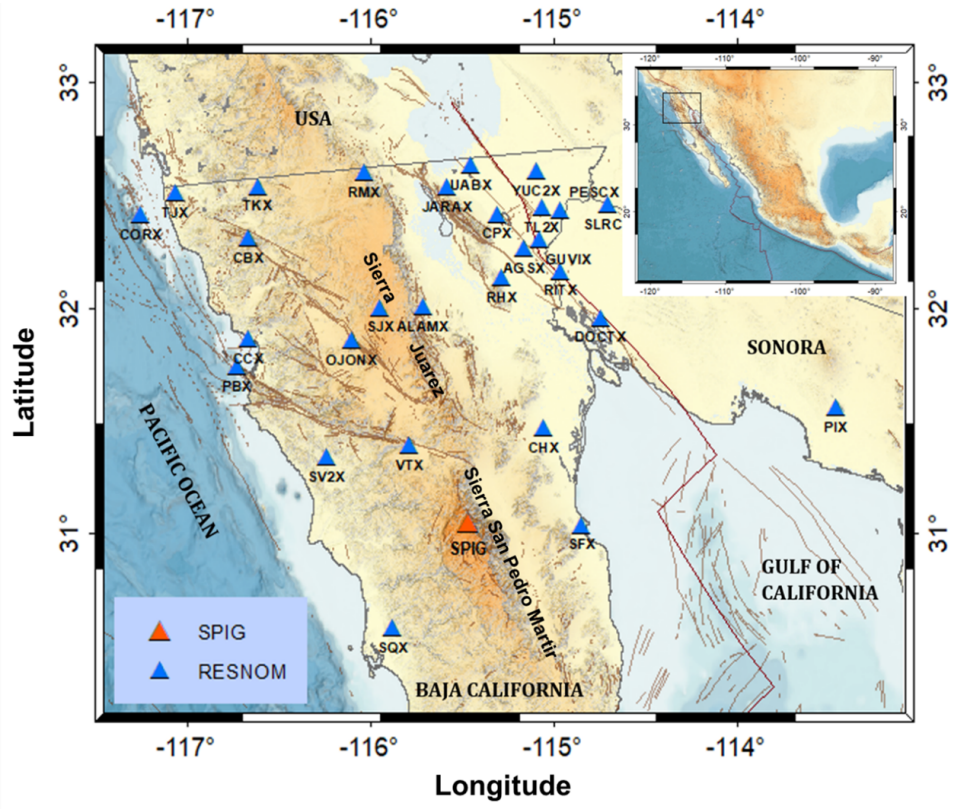

Figure 1 Seismological stations of the RESNOM seismic network in north-western Mexico. The SPIG station belongs to the SSN network. The small map shows the north part of Baja California. The main fault systems are shown.

The V_{S30} was the first parameter used to define site classes and site coefficients to estimate site-dependent response spectra (Borcherdt, 1992, 1994). Nowadays, the V_{S30} is a well-accepted and robust parameter used to characterize local site response (Hollender et al., 2018; Sairam et al., 2019; Ramírez et al., 2020; Cultrera et al., 2021). Another parameter is the engineering bedrock H_{eng_bed} (Cultrera et al., 2021), which corresponds to the depth where V_S reaches a value of 800 m/s or 1.5 km/s (EC8, 2004; Luzi et al., 2011; Bergamo et al., 2021; Bard, 2021; Giulio et al., 2021). According to Cadet et al. (2012a), the combination of different site-condition parameters, also known as proxies (Cultrera et al., 2021), results in a better soil characterization.

In a previous study, Castro et al. (2001) analyzed the site conditions of the RESNOM network when it was composed only of eight stations. These authors reported significant site effects on one of the stations, due probably to the near-surface geological conditions or topography. Since then, the network has grown to its present state, with 27 broad-band stations located mainly on rock (see Table S1, supplementary material, and Figure 1), and has steadily improved the data quality and resolution (Zúñiga and Castro, 2005). However, as with most seismic networks worldwide, the characterization of the site conditions has been somewhat overlooked (Cultrera et al., 2021; Giulio et al., 2021).

In this work, we define the site characteristics of every station of the RESNOM seismic network. Using seismic noise data, we estimate the proxies V_{S30} and H_{eng_bed}, and obtain the parameters f_0 and A_0.

2 RESNOM Seismic Stations

RESNOM currently operates with 27 stations. Each station is equipped with three-component broad-band seismographs (Table S1) and acceleration sensors with continuous recording. The seismic instrumentation is installed in two types of stations: container-type and booth-type (CICESE, 1980). All stations feature thermal insulation and are positioned on concrete bases. The map in Figure 1 shows the location of the RESNOM stations. The northern part of Baja California consists of two geological regions: the granitic Peninsular Ranges (Krummenacher et al., 1975; Gastil; Ramírez et al., 2019) and the sedimentary environment of the Mexicali Valley (Vidal-Villegas et al., 2018; Ramírez et al., 2019). A major description of geology can be found in Gastil et al. (1975), Krummenacher et al. (1975), Gastil, and Kimbrough et al. (2001). Table S1 provides information on the station's location, dynamic range, frequency response, and geological site for the broad-band instruments.

3 Methdology

The analysis was performed using only the broad-band seismometers. We consider two-hour of seismic noise recorded on Sunday, June 6th, 2021. We chose this day for having a low anthropogenic seismic noise contribution. For the pre-processing, every seismic trace was detrended, baseline corrected, tapered, and bandpass filtered between 0.05 and 35 Hz. For the analysis, we consider 30 s length windows, which were automati-

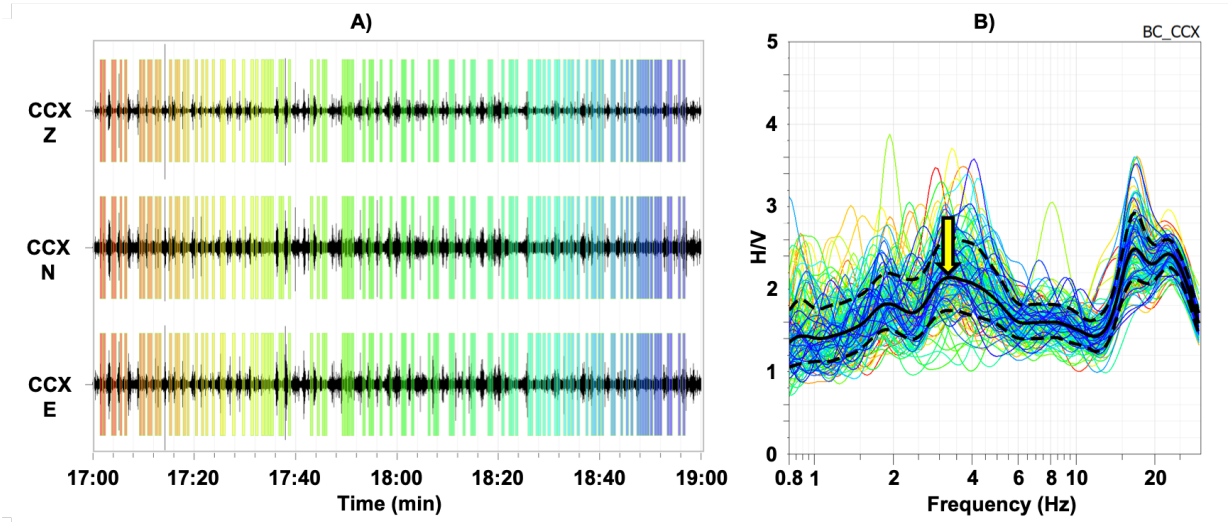

Figure 2 A) Example of seismic noise signals for the three motion components at station CCX. The color rectangles indicate the selected windows with an STA/LTA algorithm and an anti-trigger filter (details within the text). B) HVSR curves calculated for all selected windows; each colored line corresponds to the time windows in A). The vertical yellow arrow indicates the f_0. The continuous black line indicates the average, and the dashed black line indicates the standard deviation.

cally selected using an STA/LTA algorithm with the following parameters: Min STA/LTA = 0.2, Max STA/LTA = 2.0. These selection parameters avoid most transients and those windows with abnormally low amplitudes (Atakan et al., 2004).

For each selected window, we calculate the Horizontal to Vertical Spectral Ratio (HVSR) curves using the root mean square value of the horizontal components (Nogoshi and Igarashi, 1971; Nakamura, 1989, 1996, 2000):

$$H(f) = \sqrt{\frac{N(f)^2 + E(f)^2}{2}} \quad (1)$$

$$HVSR(f) = \frac{H(f)}{V(f)} \quad (2)$$

where *N(f)*, *E(f)*, and *V(f)* are the spectra of the North-South, East-West, and Vertical motion components, respectively.

We applied the Horizontal to Vertical Time Frequency Analysis (HVTFA, Fäh et al., 2009), originally proposed by Kristekova (2006), which is a module in the GEOPSY software (Wathelet et al., 2020). HVTFA employs a continuous wavelet transform based on modified Morlet wavelets (Lardies and Gouttebroze, 2002) to transform the three signal component into the time-frequency domain (Knapmeyer-Endrun et al., 2017).

Figure 2A shows an example of the seismic noise signals for the three motion components at station CCX (Figure 1). The colored rectangles indicate the selected windows considering the above-described parameters. Figure 2B shows the HVSR curves obtained for each time window, using a Konno-Ohmachi smoothing at 40. The colored lines indicate the HVSR curve for every 30-second window, the continuous black line indicates the average, and the dotted black lines indicate the standard deviation. Our objective is focused on defining shallow conditions; therefore, we considered frequencies ≥ 0.8 Hz.

Usually, the resonance frequency f_0 at sites with high impedance contrast appears as a sharp peak in the HVSR curves (Bonnefoy-Claudet et al., 2006a,b; Lermo and Chávez-García, 1993, 1994a,b; Nakamura, 1989, 1996). The fundamental frequency corresponds to the first low-frequency peak with amplitude >2 (Cadet et al., 2012b). For seismological network stations, in the ideal conditions (installed on rock sites) high impedance contrast is not expected; therefore, we do not expect sharp peaks within the HVSR curve. The high impedance contrasts (presence of sediments) between subsurface layers generally manifest as sharp peaks in the HVSR curve. However, this methodology can also be applied to obtain an accurate estimation of f_0 and A_0 (SESAME, 2004). Also, it is very important to keep clear the difference between the maximum amplitude observed in the HVSR peaks and the site amplification. Many times, it is an accurate reference to define the amplification in a site, related to a specific frequency (main peak of the HVSR curve), however, it is not as simple as directly the value of the maximum amplitude of the HVSR ratio (Bonnefoy-Claudet et al., 2006a).

Some authors assume that the HVSR curve is related to the ellipticity of Rayleigh waves and that the observed features on the HVSR curves (amplitude, peaks, etc.) can be directly related to the discrepancies on the ellipticity curves and, therefore, with heterogeneities of the subsoil (Bard, 1999; Malischewsky and Scherbaum, 2004; Malischewsky et al., 2010; Zor et al., 2010; Tuan et al., 2011; Flores et al., 2013). Furthermore, the complete HVSR curve can be inverted to estimate the variation of the V_S with depth, *i.e.*, the shear wave velocity profile (Malischewsky and Scherbaum, 2004; Malischewsky et al., 2010; Zor et al., 2010; Tuan et al., 2011; Flores et al., 2013; Wathelet et al., 2020).

We consider a three-stage inversion scheme: (1) development of the target inversion, *i.e.*, calculate the HVSR curve for each station, explained before and results shown in Figure 2; (2) parametrization, *i.e.*, an ini-

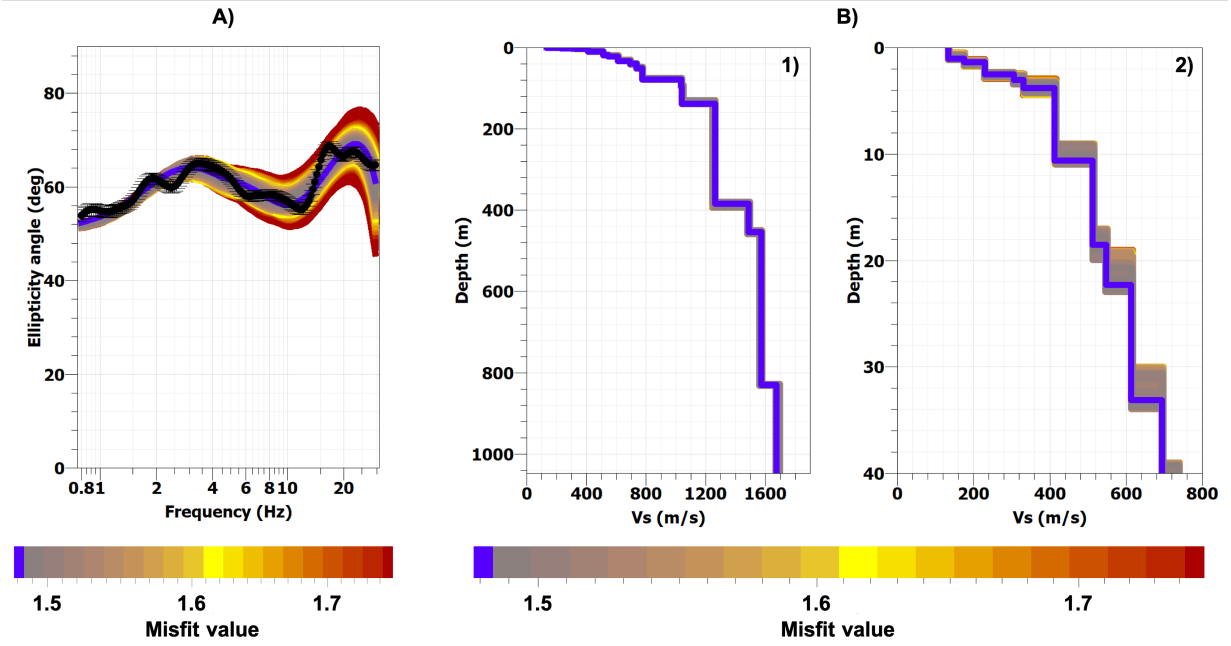

Figure 3 A) In the dark line, the HVSR averaged curve, in colors, the ellipticity curves for the inverted models. The color scale represents the misfit values. B) V_S (1) model and V_S (2) model at 40 m depth for CCX station. The solid blue line represents the velocity model with the minimum value of misfit.

Station	No. Windows	f_0 (Hz)	A_0	min. misfit	V_{S30} (m/s)	H_{eng_bed} (m)
AGSX*	106	1.131	3.3	1.08	535	42
ALAMX	85	2.203	2.4	0.93	417	165
CBX	108	1.559	3.2	1.04	470	96
CCX	99	3.437	2.1	1.48	614	78
CHX	153	0.566	1.6	0.96	392	462
CORX	17	4.292	2.4	1.26	575	77
CPX*	200	1.638	6.8	1.44	473	88
DOCTX*	110	1.103	1.8	0.51	383	293
GUVIX*	128	1.025	2.7	0.85	249	926
JARAX*	147	0.951	3.7	1.07	249	306
PBX	132	3.437	4.5	1.49	577	38
PESCX*	134	1.050	3.0	0.82	319	247
PIX**	92	0.841	1.6	0.73	213	450
RHX*	42	2.373	1.2	1.04	251	925
RITX*	117	1.103	2.5	0.61	360	206
RMX	95	1.764	2.0	1.15	495	122
SFX	166	3.793	2.1	1.17	276	841
SJX	151	9.696	7.5	0.86	958	23
SLRCX*	122	0.951	2.2	0.85	520	212
SPIG	143	9.696	1.6	0.74	405	838
SQX	142	2.963	2.2	0.94	380	138
SV2X	91	7.763	2.0	0.98	297	850
TJX	197	0.365	1.7	0.71	260	333
TKX	90	4.856	2.5	0.85	383	695
TL2X*	147	1.000	2.7	0.93	454	147
UABX*	159	0.762	2.9	0.70	173	----------
VTX	71	5.360	3.8	0.84	539	39
YUC2X*	129	0.928	2.9	0.80	426	166

Table 1 Number of windows to obtain the HVSR curve, the fundamental frequency f_0, the average amplitude at f_0 (A_0), the minimum misfit between observed and synthetic HVSR curves (adjustment of ellipticity curve), V_{S30}, and H_{eng_bed} depth for the RESNOM stations. The stations marked with * belong to the Mexicali Valley region, the rest to the Peninsular. The PIX station (**) corresponds to Sonora province.

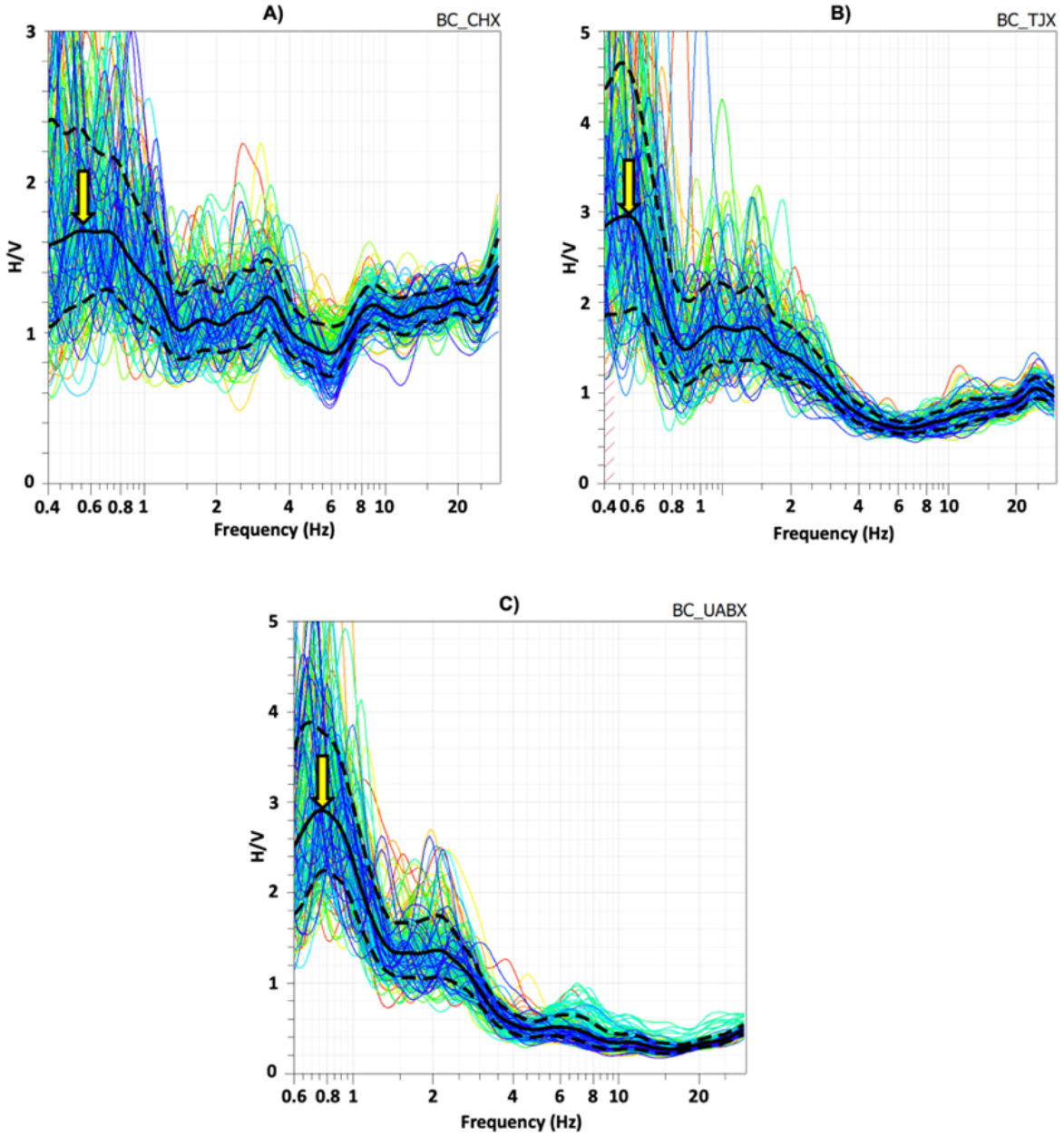

Figure 4 HVSR curves for A) CHX, B) TJX, and C) UABX stations. The continuous black line indicates the average, and the dashed black line is the standard deviation. Vertical yellow arrows indicate the f_0.

tial 1D multilayered velocity model, defined by thickness H, mass density ρ, shear velocity V_S, and compressional velocity V_P for each layer, starting with a simple and wide open velocity and depth model, using at first the higher frequencies to model the near surface layers, adding more layers at depth to model the peaks with lower frequencies; and (3) the selection of the tuning parameters inversion, number of initial models, number of iterations, number of models per iteration, and number of models to consider when resampling (Vantassel and Cox, 2021).

The inversion of the HVSR curves is performed with an iterative process, starting from the initial model proposed in stage two. The parameters are modified in each iteration to reach the smallest misfit between the observed HVSR and the theoretical curves calculated for each shear wave velocity profile (Xia et al., 2003). This misfit is calculated based on the following equation (Arintalofa et al., 2020):

$$\text{misfit} = \sqrt{\frac{1}{N}} \cdot \sum_{i=1}^{N} \left(\frac{D_i - M_i}{\sigma_i} \right)^2 \tag{3}$$

where N is the number of data points from the HVSR curve, D_i is the data resulting from inversion, M_i is the soil structural model appropriate to the parameter input on the reference model, and σ_i is the error of data measurement. A misfit one unity value represents that the predicted data fit to the observed data one standard deviation, in average (Gosselin et al., 2022), which means how far the generated model is from the observed data (Wathelet et al., 2008). Since D_i, M_i, and σ_i have the same units, the misfit is non-dimensional.

The sensitivity of the inversion procedure is closely

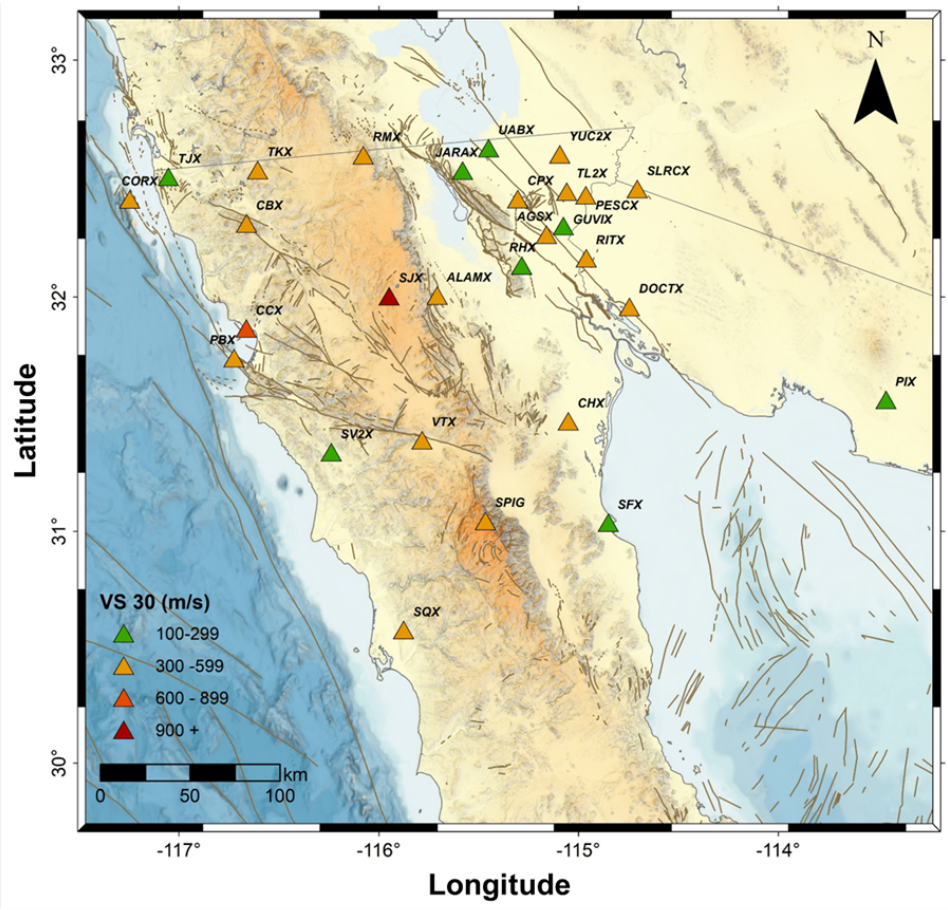

Figure 5 Broad-band seismological stations of the RESNOM seismic network and the V_{S30} values obtained for each station.

related to the frequencies and wavelengths that can be evaluated. Higher frequencies provide information about shallower subsurface layers with greater resolution due to shorter wavelengths. In contrast, lower frequencies are sensitive to deeper structures because of their longer wavelengths. In this work, we observed that the ellipticity curve exhibits a peak at low frequencies, indicating a significant impedance contrast at greater depths (~1000 m). The inversion of the HVSR curves is performed in the complete frequency domain, *i.e.*, all frequencies obtained from the HVSR curve calculation are considered.

The inversion technique used can fit the HVSR curve with multiple different models. This is a well-known issue in geophysical inversions, where different combinations of model parameters can produce similar fits to the observed data, leading to non-uniqueness in the solutions. It is often necessary to incorporate priori information or constraints on V_S values to mitigate this uncertainty. These constraints can come from independent measurements, such as borehole data, or from well-established geological and geophysical knowledge of the area under study. By integrating these additional constraints, we can narrow down the range of possible models and improve the reliability of the inversion results. In our analysis, we carefully considered the potential trade-offs and incorporated available constraints on V_S to enhance the robustness of our models. As we only have geological information, we seek to correlate the velocity models obtained with ranges of values consistent with the present lithology.

Figure 3 shows the results of this procedure for the CCX station. Figure 3A shows in solid black line the average of the observed HVSR curves (Figure 2B) and the colored lines the HVSR curves of each inverted model; the color scale refers to the misfit between these two. Figure S-1 (supplementary material) shows the fit for each station. Figure 3B shows the inverted velocity profiles at 1) full depth and 2) more detailed down to 40 m depth.

From the full-depth inverted velocity profiles V_S, we define the depth of the engineering bedrock H_{eng_bed} (Cultrera et al., 2021)—that is, the depth where V_S reaches a value of 800 m/s (EC8, 2004; Luzi et al., 2011; Bergamo et al., 2021). The more detailed profiles, down to 40 m depth, were used to obtain the value of V_{S30}, *i.e.*, the average velocity of the shear wave in the first 30 m depth in each 1D V_S profile.

4 Results and Discussion

Table 1 summarizes the results obtained for each station (f_0, A_0, V_{S30}, and H_{eng_bed}); it also shows the number of time windows used for the analysis and the minimum misfit obtained by the iterative inversion of the HVSR curves.

For most stations, the fundamental frequency exceeds 0.8 Hz except for the CHX, TJX, and UABX, which show fundamental frequencies below 0.8 Hz (Figure 4),

Stations	Site Class	V_{S30} range (m/s)
-	A (Hard rock)	>1524
SJX	B (Medium hard rock)	914 - 1524
-	BC (Soft rock)	640 - 914
AGSX, CBX, CCX, CORX, CPX, PBX, RMX, SLRCX, TL2X, VTX	C (Very dense sand or hard clay)	442 - 640
ALAMX, CHX, DOCTX, PESCX, RITX, SPIG, SQX, TKX, YUC2X	CD (Dense sand or very stiff clay)	305 - 442
GUVIX, JARAX, RHX, SFX, SV2X, TJX	D (Medium dense sand or stiff clay)	213 - 305
PIX, UABX	DE (Loose sand or medium stiff clay)	152 - 213
-	E (Very loose sand or soft clay)	< 152

Table 2 Site classification for the RESNOM stations in terms of V_{S30}, according to NEHRP (2020).

Figure 6 Photograph showing the weathered rock outcrop where the RHX station is located (Courtesy of RSC).

the first two located in the Peninsular region and the last one in the Mexicali region (Figure 1). However, the standard deviation below 0.8 Hz is higher, and the values could be considered less reliable. The frequencies seem to be concentrated between 0.365 Hz to 5.360 Hz. Out of this range are SJX and SPIG, located in Sierra Juarez and Sierra San Pedro Martir, respectively, and SV2X on the Pacific side, all of these stations located in the Peninsular region (Table 1 and Figure 1).

The geology of the SJX site consists of granodiorite (Table S1), which explains the inferred fundamental frequency of 9.696 Hz. We found the same fundamental frequency for the SPIG station (Table 1), located on metamorphic gneiss (Figure 1 and Table S1). However, for this site, the estimated value of the V_{S30} velocity (405 m/s) was lower than the one determined for SJX (958 m/s) (Figure 5). The frequencies range varies from 0.762 Hz – 2.373 Hz and from 0.365 Hz to 9.696 Hz for Mexicali and Peninsular regions, respectively.

The amplitude A_0 for most RESNOM stations is between 1.2 and 3.8. The stations out of this range define a profile from the Pacific to the deformation zone, PBX on the Pacific side, SJX in Sierra Juarez, and CPX located in the deformation zone. From Figure S-2 (supplementary material), we can observe that the thickness of the sediments is major in the deformation zone than those in the Pacific side and minor in the Sierra Juarez, at least for these stations. The values found for A_0 agree with those reported by Ávila Barrientos and Castro (2016). The authors reported A_0 values between 1.5 and 13 from HVSRs with seismic records. The range of A_0 is 1.2 to 6.8 and 1.6 to 7.5 for the Mexicali and Peninsular regions, respectively.

We observed that the V_{S30} value for the stations located in the Mexicali Valley ranges from 173 m/s (UABX station) to 535 m/s (AGSX station) (Figure 5). While for the Peninsular region, the V_{S30} value varies from 260 m/s (TJX station) to 958 m/s (SJX station) (Figure 5). The results found show a great dispersion, which corresponds with the heterogeneity of the region. The V_{S30} values defined by our seismic noise analysis are in good agreement with the existing description of the geology. The minimum V_{S30} values correspond to places located on sediments, *e.g.*, The TJX station (city of Tijuana) located on poorly consolidated sediments (Delgado-Argote et al., 1996; Ávila Barrientos et al., 2023) (Figure 5), and in opposite the higher values are in rock as the SJX station (Figure 5), located in the north-central part of Baja California (Sierra Juárez, Figure 1). Figure S-2 (supplementary material) shows the V_{S30} profiles for each station.

According to the V_{S30} values obtained for each station and the soil classification defined by NEHRP (2020) indicates that most stations are classed as type C and CD, meaning dense sand or hard clay and dense sand or very stiff clay, respectively (Table 2). However, according to the lithology RHX station, it is in intrusive igneous acid rock (Table S1, Figure 5), but the results show that the subsoil corresponds to sediments (Tables 1 and 2). This can be explained because the rock in the site is weathered, as can be observed in Figure 6. Due to the weathered rock, different sites located on rock have properties more similar to sediments than healthy rock.

The H_{eng_bed} depth for the Peninsular region varies from 23 to 850 m; the minimum depth belongs to the SJX station, which also has the highest V_{S30} value (Figure 5), while the maximum depth was found for the SV2X (V_{S30} = 297 m/s, Figure 5). In the Mexicali region, we found the shallow value for the AGSX station (42 m), which has the highest V_{S30} value in the region (Figure 5), and the maximum depth value was found for neighbor station GUVIX (926 m); however, our inverted models for the UABX station do not reach the H_{eng_bed} depth, suggesting a H_{eng_bed} depth greater than 1.1 km. The two neighbor stations, GUVIX and AGSX, show different H_{eng_bed} depths, which we speculate could be related to the heterogeneity in the zone due to the crust deformation by the interaction between the North American and Pacific

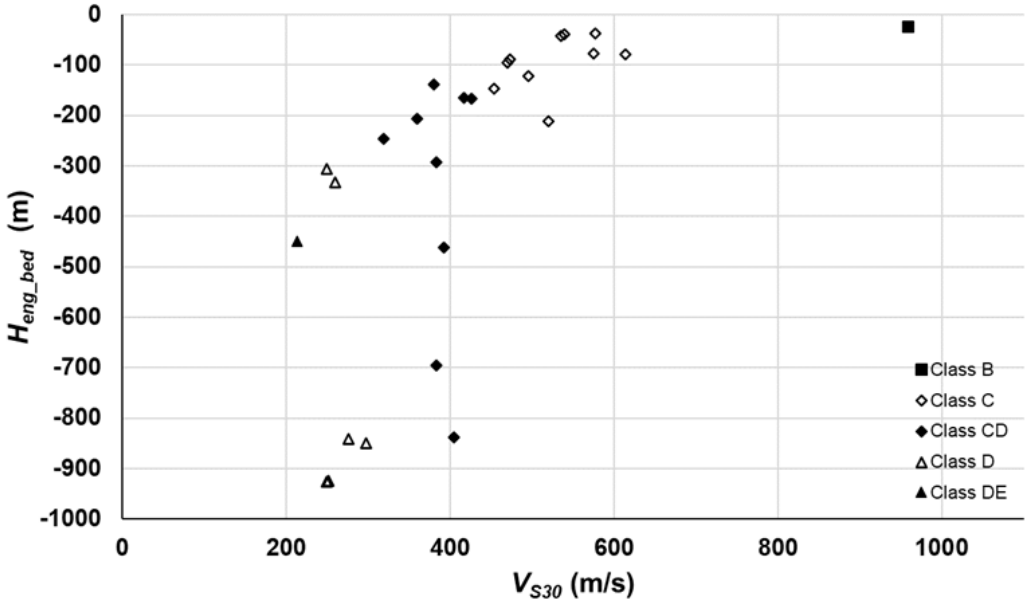

Figure 7 H_{eng_bed} versus V_{S30} for all stations. Different symbols represent the site classification based on the V_{S30} value following NEHRP (2020), shown in Table 2.

plates.

Most of the stations classified as C type (Table 2) have H_{eng_bed} depths <100 m; the rest of the stations (RMX, SLRCX, and TL2X), which represent the 30% of the C type, show depths <250 m. Most of the stations (66.66%) classified as CD have depths between 138 and 293 m. The deeper parameter is found for the SPIG station, located in Sierra San Pedro Martir (metamorphic gneiss, Table S1; Figure 1), with 838 m, where we speculate the rock is fractured, which could reduce the seismic velocity. This station is among those with the deepest H_{eng_bed} values: GUVIX (926 m), RHX (925 m), SFX (841 m), SV2X (850 m), and TKX (695 m), the first two belong to the Mexicali and the rest to the Peninsular regions. From Figure 7, it is possible to observe that these stations have V_{S30} velocities between 249 and 405 m/s. We also can observe a logic inverse trend for the shallow 400 m so that when the V_{S30} increases, the H_{eng_bed} becomes shallower.

5 Conclusions

This study, utilizing seismic noise analysis and HVSR curves inversion, represents the first attempt to provide the values of the main proxies for all the RESNOM stations. The proxies f_0 and A_0 agree with the expected values for seismological stations located on healthy rock. The soil classification from the V_{S30} proxy corresponds to the description of the geology of each station; this supports and validates our results and the use of seismic noise for obtaining proxies for seismic networks. The study enabled us to determine that the healthy properties of the rock at the RHX station are lost due to weathering.

The sediment thickness plays an important role in the amplification site since no relationship is observed between frequency and amplification. Based on the values obtained for the main proxies, the SJX station shows a relationship among different proxies, increasing frequency as increases A_0 and V_{S30}, and showing shallow depth for H_{eng_bed}; Thereafter, the SJX station can be considered a reference station for future studies.

The Mexicali and Peninsular regions show differences among parameters, particularly for high parameter values. These differences can also be observed within each region, which supports the heterogeneity of the zone due to the interaction of the North American and Pacific plates.

Given their potential implications for seismic hazard assessments, a more local and exhaustive analysis in areas presenting V_{S30} values lower than 300 m/s is strongly recommended. The use of different analysis methods or other geophysical surveys (e.g., MASW and geoelectric) will help to better constrain the parameters that we define with this first approach.

Acknowledgements

The work of LA-B was supported by the *Investigadoras e Investigadores por México* CONAHCYT program, project 2602 (before Cátedras CONACyT). Thanks to Antonio Mendoza for his technical support. Our special gratitude goes to the CICESE seismic network (RSC) group and the National Seismological Service (SSN), particularly to Víctor Hugo Espíndola. Thanks to the two anonymous reviewers and the editor Pablo Heresi.

Data Availability

Datasets related to this article can be requested from CICESE (https://resnom.cicese.mx/) and SSN (http://www.ssn.unam.mx/).

Competing Interests

The authors declare that there are no conflicts of interest or competing interests.

References

Arintalofa, V., Yuliyanto, G., and Harmoko, U. Subsurface characterization of Diwak-Derekan geothermal field by HVSR analysis method based on microtremor data. *AIP Conference proceedings*, 2296:020057, 2020. doi: 10.1063/5.0030356.

Atakan, K., Bard, P.-Y., Kind, F., Moreno, B., Roquette, P., Tento, A., and Team, S. J-SESAME: a standardized software solution for the h/v spectral ratio technique. In *13th World Conference on Earthquake Engineering*, Vancouver, B.C., Canada, 2004.

Bard, P.-Y. Microtremor Measurements: A Tool for site effect estimation? In Irikura, K., Okada, and Sasatani, editors, *The Effects of Surface Geology on Seismic Motion*, page 1251–1279. 1999.

Bard, P.-Y. Physics-based site-amplification prediction equations: a dream at reach? In *6th IASPEI/IAEE International Symposium: Effects of Surface Geology on Seismic Motion*, 2021.

Bergamo, P., Perron, V., Hammer, C., Faeh, D., and Panzera, F. Assessing the Sensitivity of Site Condition Parameters towards seismic local Amplification and their potential Use for Site Response Prediction. In *17th Swiss Geoscience Meeting, Fribourg*, page 2, 2019. doi: 10.3929/ETHZ-B-000390366.

Bergamo, P., Hammer, C., and Fah, D. On the relation between empirical amplification and proxies measured at swiss and japanese stations: systematic regression analysis and neural network prediction of amplification. *Bulletin of the Seismological Society of America*, 111(1):101–120, 2021.

Bonnefoy-Claudet, S., Cornou, C., Bard, P.-Y., Cotton, F., Moczo, P., Kristek, J., and Fäh, D. H/V ratio: a tool for site effects evaluation. Results form 1-D noise simulation. *Geophysical Journal International*, 167, 2:827–837, 2006a. doi: 10.1111/j.1365-246X.2006.03154.x.

Bonnefoy-Claudet, S., Cotton, F., and Bard, P.-Y. The nature of noise wavefield and its applications for site effects studies. *Earth Science Reviews*, 79:3–4, 205–227, 2006b. doi: 10.1016/j.earscirev.2006.07.004.

Borcherdt, R. Simplified site classes and empirical amplification factors for site-dependent code provisions. In *NCEER, SEAOC, BSSC workshop on site response during earthquakes and seismic code provisions, Univ*. Southern California, Los Angeles, California, 1992.

Borcherdt, R. Estimates of site-dependent response spectra for design (methodology and justification. *Earthquake Spectra*, 10 (4):617–653, 1994.

Cadet, H., Bard, P.-Y., Duval, A., and Bertrand, E. Site effect assessment using KiK-net data: Part 2—Site amplification prediction equation based on f 0 and VSZ. *Bulletin of Earthquake Engineering*, 10:451–489, 2012a.

Cadet, H., Bard, P.-Y., and Rodriguez-Marek, A. Site effect assessment using KiK-net data: Part 1— A simple correction procedure for surface/downhole spectral ratios. *Bulletin of Earthquake Engineering*, 10:421–448, 2012b.

Castro, R., Mendoza, L., Inzunza, L., and Group, R. Microtremor observations from the seismic network RESNOM of Baja California, Mexico. *Bolletino di Geofisica Teorica ed Applicata*, 42:245–254, 2001.

CICESE. Centro de Investigación Científica y de Educación Superior de Ensenada (CICESE) Ensenada Baja California, México. In *Red Sísmica del Noroeste de México*. 1980. doi: 10.7914/SN/BC.

Cornou, C. and Bard, P.-Y. *Seismology and Earthquake Engineering Research Infrastructure Alliance for Europe – SERA, European strong ground motion characterization road map. WP7 Networking databases of site and station characterization*. ETH Department of Earth Sciences, 2019.

Cultrera, G., Cornou, C., Giulio, G., and Bard, P.-Y. Indicators for site characterization at seismic station: recommendation from a dedicated survey. *Bulletin of Earthquake Engineering*, 19: 4171–4195, 2021. doi: 10.1007/s10518-021-01136-7.

Delgado-Argote, L., Hinojosa-Corona, A., Aragón-Arreola, M., and Frías-Camacho, V. Estudio de riesgo reológico en Tijuana, Baja California con base en rasgos estructurales y la respuesta del terreno. *GEOS*, 16(2):57–89, 1996.

EC8. Eurocode 8: design of structures for earthquake resistance - Part 1: General rules, seismic actions and rules for buildings, EN 1998-1, Draft 6, Doc CEN/TC250/SC8/N335, European Committee for Standardization (CEN, 2004.

Flores, H., Malischewsky, P., and Jentzsch, G. H/V spectral ratio analysis and Rayleigh modelization in Eastern Thuringia, Germany. *Geofísica Internacional*, 52-4:355–364, 2013.

Flores-Estrella, H. Métodos alternos para la estimación del efecto de sitio a partir de registros de microtremores. In *División de Estudios de Ciencias de la Tierra, Facultad de Ingeniería, UNAM. Bachelor Thesis*. In Spanish, 2001.

Fäh, D., Wathelet, M., Kristekova, M., Havenith, H., Endrun, B., Stamm, G., Poggi, V., Burjanek, J., and Cornou, C. Using ellipticity information for site characterisation. Technical report, 2009. D4, final report EC project number: 026130, NERIES JRA4 "Geotechnical Site Characterisation", task B2.

Gastil, G. Terranes of peninsular California and adjacent Sonora.

Gastil, R., Phillips, R., and Allison, E. *Reconnaissance Geology of the State of Baja California*. Geological Society of America, 1975. doi: 10.1130/MEM140-p1.

Giulio, G., Cultrera, G., Cornou, C., Bard, P.-Y., and Al Tfaily, B. Quality assessment for site characterization at seismic stations. *Bulletin of Earthquake Engineering*, 19:4643–4691, 2021. doi: 10.1007/s10518-021-01137-6.

Gosselin, J., Dosso, S., Askan, A., Wathelet, M., Savvaidis, A., and Cassidy, J. A review of inverse methods in seismic site characterization. J Seismol 26, 2022.

Hauksson, E., Helmberger, D., Hutton, K., Kanamori, H., Wei, S., Yang, W., Vidal, A., Munguía, L., Díaz, G., and Farfán, F. Preliminary seismotectonic synthesis of the 2010 Mw7. In *2 El Mayor-Cucapah earthquake sequence*. Baja California, 2010.

Hollender, F., Cornou, C., Dechamo, A., Oghalaei, K., Renalier, F., and Maufroy, E. Characterization of site conditions (soil class, VS30, velocity profiles) for 33 stations from the French permanent accelerometric network (RAP) using surface wave methods. *Bulletin of Earthquake Engineering*, 16:2337– 2365, 2018. doi: 10.1007/s10518-017-0135-5.

Kimbrough, D., Smith, D., Mahoney, J., Moore, T., Grove, M., Gastil, R., Ortega-Rivera, A., and Fanning, C. Forearc-basin sedimentary response to rapid Late Cretaceous batholith emplacement in the Peninsular Ranges of southern and Baja California. *Geological Society of America*, 29(6):491–494, 2001.

Knapmeyer-Endrun, B., Golombek, M., and Ohrnberger, M. Rayleigh Wave Ellipticity Modeling and Inversion for Shallow Structure at the Proposed InSight Landing Site in Elysium Planitia. *Mars. Space Sci*, Rev 211:339–382, 2017. doi: 10.1007/s11214-016-0300-1.

Kristekova, M. Time-frequency analysis of seismic signals, 2006.

Krummenacher, D., Gastil, R., Bushee, J., and Doupont, J. K-Ar Apparent Ages, Peninsular Ranges Batholith, Southern California

and Baja California. *Geological Society of American Bulletin*, V. 86(50605):760–768„ 1975.

Lardies, J. and Gouttebroze, S. Identification of modal parameters using the wavelet transform. *Int. J. Mech*, Sci. 44:2263–2283, 2002.

Lermo, J. and Chávez-García, F. Site effect evaluation using spectral ratios with only station. *Bulletin of the Seismological Society of America*, 83(5):1574–1594, 1993.

Lermo, J. and Chávez-García, F. Site effect evaluation at Mexico City: dominant period and relative amplification from strong motion and microtremor records. *Soil Dynamics and Earthquake Engineering*, 13:413–423, 1994a.

Lermo, J. and Chávez-García, F. Are Microtremors Useful in Site Response Evaluation? *Bulletin of the Seismological Society of America*, 84(5):1350–1364, 1994b.

Luzi, L., Puglia, R., Pacor, F., Gallipolli, M., Bindi, D., and Mucciarelli, M. Proposal for a soil classification based on parameters alternative or complementary to Vs30. *Bulletin of Earthquake Engineering*, 9:1877–1898, 2011. doi: 10.1007/s10518-011-9274-2.

Malischewsky, P. and Scherbaum, F. Love's formula and H/V-ratio (ellipticity) of Rayleigh waves. *Wave motion*, 40:57–67, 2004.

Malischewsky, P., Zaslavsky, Y., Gorstein, M., Pinsky, V., Tran, T., Scherbaum, F., and Flores-Estrella, H. Some new theoretical considerations about the ellipticity of Rayleigh waves in the light of site effect studies in Israel and Mexico. *Geofísica Internacional*, 49:141–152, 2010.

Nakamura, Y. A Method for Dynamic characteristics Estimation of Subsurface using Microtremors on the Ground Surface. *Quarterly Report of Railway Technical Research Institute (RTRI*, 30:1, 1989.

Nakamura, Y. Real-time information systems for hazards mitigation. In *Proceedings of the 11th World Conference on Earthquake Engineering*, Acapulco, Mexico, 1996.

Nakamura, Y. Clear Identification of fundamental idea of Nakamura's technique and its applications. In *12 World Conference of Earthquake Engineering*, New Zealand, 2000.

NEHRP. NEHRP (National Earthquake Hazards Reduction Program) Recommended seismic provisions for new buildings and other structures (FEMA P-2082-1. In *Provisions and Part 2 Commentary. Building Seismic Safety Council of The National Institute of Buildings Sciences. Federal Emergency Management Agency*, volume 1, Part 1. Washington, D.C, 2020.

Nogoshi, M. and Igarashi, T. On the amplitude characteristics of microtremor (Part 2. *Journal Seismological Society Japan*, 24: 26–40, 1971.

Ramírez, A., Flores, H., Preciado, A., Bandy, W., Lazcano, S., Alcántara, L., Aguirre, J., and Korn, M. Subsoil classification and geotechnical zonation for Guadalajara City, México: Vs30, soil fundamental periods, 3D structure and profiles. *Near Surface Geophysics*, 18, 2:175–188, 2020. doi: 10.1002/nsg.12085.

Ramírez, E., Vidal-Villegas, J., Nuñez-Leal, M., Ramírez-Hernández, J., A., M.-T., and E, R.-V. Seismic Noise Levels in Northern Baja California, Mexico. *Bulletin of the Seismological Society of America*, 109(2):610–620, 2019. doi: 10.1785/0120180155.

Sairam, B., Singh, A., Patel, V., Chopra, S., and Ravi Kumar, M. VS30 mapping and site characterization in the seismically active intraplate region of Western India: implications for risk mitigation. *Near Surface Geophysics*, 17:533–546, 2019. doi: 10.1002/nsg.12066.

SESAME. Guidelines for the implementation of the H/V spectral ratio technique on ambient vibrations. *Measurements, processing and interpretation SESAME European research project*, 2004.

Tramelli, A., Galluzzo, D., Del Pezzo, E., and Vito, M. A detailed study of the site effects in the volcanic area of Campi Flegrei using empirical approaches. Geophysical. *Journal International*, 182(ue 2):1073–1086, 10 1111 1365–246 2010 04675, 2010.

Tuan, T., Scherbaum, F., and Malischewsky, P. On the relationship of peaks and troughs of the ellipticity (H/V) of Rayleigh waves and the transmission response of single layer over halfspace models: Relationship of peaks and troughs of H/V-ratio. *Geophysical Journal International*, 184:793–800, 2011. doi: 10.1111/j.1365-246X.2010.04863.x.

Vantassel, J. and Cox, B. SWinvert: a workflow for performing rigorous 1-D surface wave inversions. *Geophysical Journal International*, 224:1141–1156, 2021.

Vidal-Villegas, J., Munguía, L., González-Ortega, J., Nuñez-Leal, M., Ramírez, E., Mendoza, L., Castro, R., and Wong, V. The Northwest Mexico Seismic Network: Real-Time Seismic Monitoring in Northern Baja California and North-western Sonora, Mexico. *Seismological Research Letters*, 89, Number 2A, 2018. doi: 10.1785/0220170183.

Wathelet, M., Jongmans, D., and Ohrnberger, M. Surface-wave inversion using a direct search algorithm and its application to ambient vibration measurements. Near surface.

Wathelet, M., Jongmans, D., Ohrnberger, M., and Bonnefoy-Claudet, S. Array performances for ambient vibrations on a shallow structure and consequences over V s inversion. Journal of Seismology, 12, 2008.

Wathelet, M., Chatelain, J.-L., Cornou, C., Giulio, G., Guillier, B., Ohrnberger, M., and Savvaidis, A. Geopsy: A User-Friendly Open-Source Tool Set for Ambient Vibration Processing. *Seismological Research*, Letters, 91(3:1878–1889, 2020. doi: 10.1785/0220190360.

Xia, J., Miller, R., Park, C., and Tian, G. Inversion of high frequency surface waves with fundamental and higher modes. *Journal of Applied Geophysics*, 52:45–57, 2003. doi: 10.1016/S0926-9851(02)00239-2.

Zor, E., Özalaybey, S., Karaaslan, A., Tapırdamaz, M., Özalaybey, S., Tarancıoğlu, A., and B, E. Shear wave velocity structure of the İzmit Bay area (Turkey) estimated from active–passive array surface wave and single-station microtremor methods. *Geophysical Journal International*, 182:1603–1618, 2010. doi: 10.1111/j.1365-246X.2010.04710.x.

Zúñiga, F. and Castro, R. The RESNOM seismic catalog and its bearing on the seismicity of North-western Mexico. *Geofísica Internacional*, 44(2):143–155, 2005. doi: 10.22201/igeof.00167169p.2005.44.2.249.

Ávila Barrientos, L. and Castro, R. Site Response of the NARS-Baja and RESBAN Broad-band Network of the Gulf of California, México. *Geofísica Internacional*, 55-2:131–154, 2016.

Ávila Barrientos, L., Yegres-Herrera, L., Aragón, A., Rodríguez-Corella, and Cruz-Berumén, A. Caracterización del deslizamiento de ladera de la colonia Vista Alamar, 2023.